Oceanologia, 67 (2)/2025, 67203
Polish Academy of Sciences
Institute of Oceanology

https://doi.org/10.5697/KAOE6308

Hydroacoustic technique for determination of the orientation of aggregated Baltic herring

Aleksander Żytko[1,*], Natalia Gorska[1,*], Dezhang Chu[2], Beata Schmidt[3,*]

Abstract
The distribution of fish orientation is a very important factor influencing their Target Strength (TS), and thus the hydroacoustic assessment of fish abundance. A technique has been developed to estimate the orientation distribution of aggregated Baltic herring (*Clupea harengus*) by fitting the TS histograms obtained from the theoretical backscattering model to the measured TS histograms. By using available morphometry data of Baltic herring, a modified resonance scattering model to describe the backscattering by Baltic herring has been developed. Using this model, TS histograms were generated for different probability density functions (PDFs) of fish orientation, and then compared with the measured TS histograms. Based on the best fit to the measured histograms, the most likely distribution of herring orientation can be inferred.

Keywords
Target Strength; Modified resonance scattering model; Fish orientation; Baltic herring

[1]*Institute of Oceanology, Polish Academy of Sciences, Powstańców Warszawy 55, 81–712 Sopot, Poland*
[2]*NOAA Fisheries, Northwest Fisheries Science Center, 2725 Montlake Blvd. E., Seattle, WA 98112, USA*
[3]*National Marine Fisheries Research Institute, ul. Kołłątaja 1, 81–332 Gdynia, Poland*
***Correspondence**: azytko@iopan.pl (A. Żytko); gorska@iopan.pl (N. Gorska); bschmidt@mir.gdynia.pl (B. Schmidt)

Received: 23 February 2024; **revised:** 4 December 2024; **accepted**: 24 February 2025

1. Introduction

Herring (*Clupea harengus*), a link between lower and higher trophic levels, plays an important role in the Baltic Sea pelagic ecosystem (Ojaveer, 1988; Wyszyński, 1997; Cardinale and Arrhenius, 2000; Grygiel et al., 2011). The assessment of the ecosystem state requires updated knowledge of the abundance of Baltic herring and its temporal and spatial variability (Grygiel and Wyszyński, 2003; von Dorrien et al., 2013). Considering that *Clupea harengus* is an economically valuable species in the Baltic countries, this knowledge is desirable for the sustainable management of Baltic fish resources (Ojaveer, 1988; Kulmala et al., 2007; von Dorrien et al., 2013; Sawicki et al., 2019; Hornborg, 2023).

Baltic herring abundance is conventionally assessed using hydroacoustic techniques in the Baltic International Acoustic Surveys (BIAS) every year (Casini et al., 2011; Grygiel et al., 2011) in line with International Council for the Exploration of the Sea (ICES) recommendations (e.g., ICES, 2017). Measured Target Strength (TS), an estimate of fish size, is needed to convert echo signals to fish abundance (Simmonds and MacLennan, 2005). A large body of literature suggests that the accuracy of fish abundance estimation depends on the accuracy of the TS value that is used to convert acoustic volume density to number density (Simmonds and MacLennan, 2005; Kasatkina, 2009; Fässler, 2010; Scoulding et al., 2017). Numerous hydroacoustic measurements (Didrikas, 2005; Didrikas and Hansson, 2004; Kasatkina, 2009; Lassen and Stæhr, 1985; Peltonen and Balk, 2005; Rudstam et al., 1988, 1999; Schmidt et al., 2011), as well as theoretical studies (Fässler et al., 2008; Fässler and Gorska, 2009; Fässler, 2010; Gorska and Idczak, 2010; Idczak and Kniaź-Kubacka, 2012; Idczak and Gorska, 2016; Gorska and Idczak, 2021), have been dedicated to Baltic herring TS. Despite this fact the most appropriate TS to total length l relationship (TS-l relationship) for use in hydroacoustic Baltic herring abundance estimation is unknown. The primary problem is that many factors that can strongly affect herring TS, e.g., depth of fish occupation and fish orientation (Fässler et al., 2008; Fässler and Gorska, 2009; Fässler, 2010; Gorska and Idczak, 2010; Idczak and Kniaź-Kubacka, 2012; Idczak and Gorska, 2016; Gorska and Idczak, 2021), were not controlled during the mentioned TS measurements. However, these factors could significantly differ in the conducted TS measurements and in acoustic abundance estimation in

BIAS cruises. Therefore, when using the measured *TS-l* regression, the estimation of herring abundance could be significantly biased. This means that factors that can strongly impact the herring backscattering properties should be controlled both when measuring the target strength of individuals and estimating herring abundance. Accounting for the effect of herring orientation on its backscattering (e.g. Gorska and Idczak, 2021), the data on herring orientation is highly desirable for proper interpretation of the hydroacoustic measurements.

Accurate information on fish orientation has been an important research issue for herring in the northeast Atlantic and the North Sea (Nakken and Olsen, 1977; Edwards et al., 1984; Blaxter and Batty, 1990; Huse and Ona, 1996; Huse and Korneliussen, 2000; Ona, 2001). It has been shown that herring orientation in schools can change substantially depending on the time of day, fish depth and behaviour (Beltestad, 1973; Blaxter and Hunter, 1982; Huse and Ona, 1996; Freon and Misund, 1999; Huse and Korneliussen, 2000). The orientation may also depend on external stimuli, such as underwater noise (Olsen et al., 1983; Vabø et al., 2002; Mitson and Knudsen, 2003; Ona et al., 2007) or predator attack (Thorne and Thomas, 1990; Nøttestad, 1998). Unlike the northeast Atlantic and the North Sea herrings, no research on orientation has been conducted for the Baltic herring. Due to differences in herring swimbladder morphometries and tissue fat contents as well as physical environment (Fässler et al., 2007, 2008; Fässler and Gorska, 2009; Teacher et al., 2013; Gorska and Idczak, 2021), results of research on herrings in the northeast Atlantic and North Sea may not be transferred directly to Baltic herring. For these reasons, an approach to estimate orientation would improve the accuracy of Baltic Herring abundance estimates.

Measuring the spatial orientation of fish is very challenging. There are a few possible ways to estimate fish orientation. The use of optical cameras is the most direct method. The first set of measurements of herring orientation in schools was carried out using optical methods (Ona,1984; Huse and Ona, 1996; Huse and Korneliussen, 2000). These methods have two important limitations: small sample volume and possible fish reactions (e.g., attraction by light source) potentially resulting in inaccurate orientation measurements (Stanton et al., 2003). Hydroacoustic methods have also been developed to determine marine animal orientation. A review of these methods is presented in Żytko (2021, Chapter 1). These methods can be categorized as direct and indirect methods. The direct methods proposed some techniques to determine fish orientation directly from the collected hydroacoustic data (Ona, 2001; Stanton et al., 2003; Burwen et al. 2007; Jaffe and Roberts, 2011). Compared to the optical techniques, the direct hydroacoustic methods are less invasive and provide a much larger sample volume, hence covering a wider study area. The direct hydroacoustic methods (Stanton et al., 2003; Burwen et al. 2007; Jaffe and Roberts, 2011) have some limitations that make their application difficult for *in situ* conditions. It is due to the need to use expensive measuring equipment (broadband echosounders and/or viewing angles) and advanced, complex analysis of the collected hydroacoustic data. The indirect, inverse hydroacoustic methods (Chu et al., 1993; Traykovski et al. 1998) require the creation of backscattering models and comparison of the obtained theoretical results with measured backscattering data to calculate the animal orientation. The analysis could be complicated because the backscattering depends on many external factors (not only orientation).

None of the above direct hydroacoustic methods can be easily applied in situ to estimate fish orientation. This stimulated us to look for a less complicated and more efficient indirect method that would allow us to use echosounder data from routine hydroacoustic measurements and apply relatively simple data analysis techniques. In this article, an inverse hydroacoustic method to infer Baltic herring orientation has been developed. The main idea of this technique is to use the well-known fact that the TS histograms for the aggregated Baltic herring depend on herring distributions over fish length, occupied depth, and the orientation of individual herring (Medwin and Clay, 1998; Fässler and Gorska, 2009; Gorska and Idczak, 2021). During the standard hydroacoustic assessment of herring abundance in BIAS cruises, the fish total length data is obtained from direct biological sampling (trawls). The TS and depth distributions of herring individuals can be extracted from the backscattering data collected just before the trawl. Using the data on herring total length and herring depth distribution for the chosen trawl, TS histograms for the aggregated Baltic herring are computed for different herring orientation distributions. Then the computed histograms are compared with the measured TS histograms for the chosen trawl. Herring orientation distribution for which the fit is the best is recognized as actual orientation distribution. A new modified resonance model has been developed to generate TS histograms for aggregated herring. The model not only allows a new look at some herring backscattering properties but also becomes the basis for the developed algorithm to infer herring orientation distribution.

2. Methodology

When developing a hydroacoustic inverse method to determine fish orientation, it is important to understand the influence of fish tilt angle distribution on the target strength (TS) distribution of aggregated fish individuals. Therefore, in this paper, we focus on solving the forward problem of the acoustic backscattering by individual Baltic herring. The aim was to deepen our theoretical understanding of the relationship between the shape of the TS histograms of Baltic herring and the distributions of their tilt angle and total length of the involved individuals.

A model is developed to calculate the TS probability density function (PDF) based on fish tilt angle and total length distributions from numerically generated aggregations of Baltic herring individuals. The approach is described in detail in the following subsections.

2.1 Numerical generation of herring aggregations

First, a hypothetical herring aggregation was generated. A random tilt angle θ (the angle of the longitudinal axis of the fish's body relative to the horizon), depth, and total length were attributed to each hypothetical fish. For each selected haul a random total length was drawn from the measured herring total length distribution. A random fish depth was taken from the depth distribution of herring individuals determined from echograms obtained just before the haul. Herring total length distributions and depth distributions of single echoes for the selected hauls are presented in Figure A1 and Figure A2, respectively. The collection of fish total length and depth data are described in subsection 2.4. For each aggregation, the number of individuals was equal to ten times the number of fish caught in the haul. The number of individuals has been increased to include more length-orientation-depth configurations. Smaller number could result in a larger random spread of results over many algorithm implementations.

The herring tilt angle follows a Gaussian or normal distribution:

$$\Phi(\theta) = \frac{1}{s_\theta\sqrt{2\pi}} e^{\left(\frac{-(\theta-\overline{\theta})^2}{2s_\theta^2}\right)} \tag{1}$$

where $\overline{\theta}$ means tilt angle and s_θ its standard deviation. Positive angle indicates the position of the fish with its head up, and negative angle for its head down.

Then, the TS for each individual fish in the generated aggregation was calculated using the TS model described in the next subsection.

2.2 Backscattering model. Its justification, description and verification

2.2.1 Modified resonance scattering model: rationale

To study numerically backscattering properties of Baltic herring (to generate TS histograms for herring aggregations) and to create a basis for applying the hydroacoustic techniques to determine orientation statistics of aggregated Baltic herring, the backscattering model is required. To choose the model we evaluated the products of the wave number k ($k = 2\pi f/c_w$, where c_w is the sound speed in water) and the characteristic swimbladder dimensions (e.g. half of swimbladder length and width), parameters controlling the regime of backscattering (Simmonds and MacLennan, 2005). We supposed that the swimbladder shape could be approximately represented by a prolate spheroid with the minor semi-axis a_{ps} and the major semi-axis b_{ps}. Taking into account the dependence between swimbladder and fish lengths (Eq. (11) below) as well as relationships between fish morphometry parameters (Eqs. (5), (8), (9), (12) below) Figure 1a has been generated. The calculations were done at the frequency of 38 kHz, at which primary herring abundance data are collected (Grygiel et al., 2011). Here a_{es}, denotes equivalent spherical radius, as it is expressed below by Eq. (5). It was shown (Figure 1a) that the kb_{ps} parameter is much greater than 1, ka_{es} is greater than 1 for fish larger than 16 cm, and ka_{ps} is close to 1 for largest fish. These parameter values suggest we cannot use directly existing resonance models (e.g. Love, 1978; Ye, 1997; Fässler, 2010; Scoulding et al., 2015, 2022), or a geometric scattering approach (e.g., Gaunaurd, 1985). Our "working area" is rather in the "transitional" regime.

This is confirmed by the dependences of Reduced Target Strength (RTS) on ka – parameter for spherical swimbladder (a is its radius), generated using two different backscattering models (Figure 1b). Here RTS is defined as:

$$RTS = TS - 20\log_{10}(a/2) \tag{2}$$

where TS is defined by Eq. (33) below. This comparative analysis demonstrated that the resonance scattering model is not consistent with the exact values of the Modal Series Solution for a sphere for ka larger than 1.3. This means that also in the case of the prolate spheroid, we should be careful when using the resonance model (Love, 1978; Ye, 1997; Fässler, 2010; Scoulding et al., 2015, 2022) for the larger parameter values we are dealing with (Figure 1a).

We considered also the possibility of application of *Modal-Series-Based Deformed Cylinder Model* (*MSB-DCM*; Stanton, 1988a,b, 1989) that has been widely used in the previous studies of the backscattering properties of the Baltic herring (Fässler et al., 2008; Fässler and Gorska, 2009; Fässler, 2010; Idczak and Gorska, 2016; Gorska and Idczak, 2021). However, it may be problematic since this approach is valid only for normal or near-normal sound incidence relative to the longitudinal straight axis of the fish body and swimbladder (Jech et al., 2015). It would limit the applicability of the hydroacoustic technique to determine the herring orientation that we would like to develop. In addition, the *MSB-DCM* is not applicable near the resonance frequency for siwmbladdered fish since it predicts incorrect resonance scattering frequencies.

The use of more precise and advanced numerical models described in Jech et al. (2015), such as the *Boundary Element Method* (BEM) by Francis (1993), Foote and Francis (2002), and Francis and Foote (2003), or *Finite Element Method* (FEM) by Zampolli et al. (2007), was not possible due to the lack of precise morphometric data for the Baltic herring swimbladder. Moreover, the challenge of applying FEM or BEM is too computationally expensive and is impossible to apply once an inversion approach, such as the

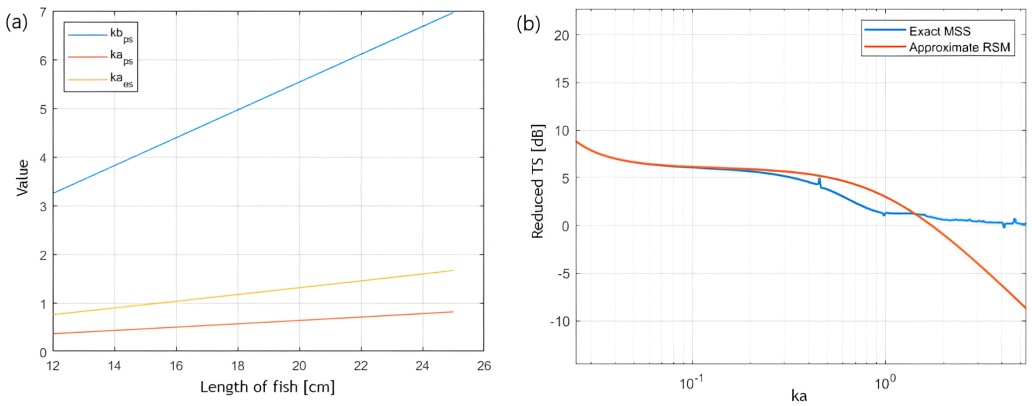

Figure 1. Dependence of product of wave number and dimension of the swimbladder to the length of the fish for the semi-major axis (blue), semi-minor axis (red) and radius of equivalent sphere (yellow) (a); the Resonance Scattering Model (*RSM*) versus exact Modal Series Solution (*MSS*) for a sphere. The cross of the two curves occurs at $ka \approx 1.3$.

one proposed in this paper, is involved.

Considering the above, we developed the model which will be the expansion of the existing resonance scattering model (Love, 1978; Ye, 1997; Scoulding et al., 2015, 2022) to much higher values of ka, where k is the acoustic wave number and a, is the characteristic swimbladder dimensions (larger fish).

2.2.2 Model description

To calculate the differential backscattering cross-section of a swimbladder $\sigma_{bs}(f,z)$, whose shape can be approximately represented by a prolate spheroid, we start with a form of the resonance scattering solution for a prolate spheroidal bubble at the normal incidence (Love, 1978; Ye, 1997; Scoulding et al., 2015, 2022). A major advantage of the resonance model is it has a closed analytical form and can be easily used in a model-based inverse algorithm. Although a resonance model conceptually is applicable only to the frequencies near the resonance frequency of swimbladder and then independent of fish orientation, we can introduce a frequency-dependent coefficient K of an analytical form to both denominator and numerator and the frequency dependent damping term $\delta(f)$ that allows the model to approach the asymptotic values of the backscattering cross-section based on the Kirchoff Approximation (Gaunaurd, 1985), an extension of the resonance scattering model to non-resonance frequency range:

$$\sigma_{bs}(f,z) = \frac{K\zeta^2 a_{es}^2}{\left[1-\left(\frac{f_{ps}}{f}\right)^2\right]^2 + \frac{K}{\delta(f)^2}} \tag{3}$$

where f is the echosounder frequency and z is the depth where the fish is present. All values and parameters in this section are expressed in SI units unless otherwise stated. The symbol f_{ps} is the resonance frequency of the prolate-spheroid-shaped swimbladder, which also depends on z. Note that Eq. (3) is applicable to much higher frequencies, or ka ranges, where the backscattering is sensitive to fish orientation and a frequency-dependent analytical term capable of adequately characterizing this orientation dependence can be easily added to our scattering model later.

The factor ζ is a coefficient accounting for the amplitude enhancement due to swimbladder elongation (Ye, 1997):

$$\zeta = \frac{\varepsilon^{-2/3}(1-\varepsilon^2)^{1/2}}{\ln\frac{1+(1-\varepsilon^2)^{1/2}}{\varepsilon}} \tag{4}$$

where ε is the ratio of the minor semi-axis a_{ps} to the major semi-axis b_{ps} of the prolate spheroid, i.e., $\varepsilon = \frac{a_{ps}}{b_{ps}}$ and it is a function of depth, z. Here $a_{es}(z)$ is the equivalent spherical radius, i.e., the radius of a sphere with a volume equal to that of the swimbladder (a prolate spheroid here) at depth z:

$$a_{es}(z) = \sqrt[3]{\frac{3}{4\pi}V(z)} = a_{ps}\,\varepsilon^{-1/3} \tag{5}$$

where $V(z)$ is the volume of the swimbladder at depth z. It relates to its volume at a sea surface $z = 0$ m, $V(0)$, according to Boyle's law (Levine, 1978):

$$V(z) = \frac{P(0)V(0)}{P(z)} \tag{6}$$

In this formula, the hydrostatic pressure $P(z)$ (in pascals) is calculated as follows (Kloser et al., 2002):

$$P(z) = (1+0.103z)\times 10^5 \tag{7}$$

where z is the depth (in meters).

The volume of a swimbladder at the sea surface is calculated as an appropriate percentage of the volume of whole fish:

$$V(0) = n\frac{w}{\rho} \tag{8}$$

where ρ is the average density of the fish, w is its mass, and n is the fish swimbladder's volume fraction (i.e., the ratio of the swimbladder volume to that of whole fish). According to Ona (1990) and Nero et al. (2004), this percentage may vary from 5% to 15%. The fish density (ρ) is calculated from the sea water density (ρ_w) as: $\rho = 1.05\rho_w$. The weight of the fish is calculated from its length based on the formula given by Kasatkina (2007):

$$w = 0.0031\, l^{3.2183} \tag{9}$$

where w is the mass in grams, l is the total fish length in centimetres.

The resonance frequency of a prolate spheroidal swimbladder f_{ps} in Eq. (3) is a function of the resonance frequency f_0 of a sphere with an equal volume (Love, 1978; Ye, 1997):

$$f_{ps} = f_0\, 2^{\frac{1}{2}} \varepsilon^{-\frac{1}{3}} (1-\varepsilon^2)^{\frac{1}{4}} \times \left\{ \ln \frac{1+(1-\varepsilon^2)^{\frac{1}{2}}}{1-(1-\varepsilon^2)^{\frac{1}{2}}} \right\}^{-\frac{1}{2}} \tag{10}$$

To determine the aspect ratio function $\varepsilon(z)$, information on the geometrical dimensions of swimbladders is needed. To calculate the length of the swimbladder at the sea surface we use the formula proposed by Gorska and Idczak (2021) for Baltic herring:

$$l_{ps} = 2\, b_{ps}(0) = 0.3596\, l - 0.2368 \tag{11}$$

where parameters $b_{ps}(0)$ and fish total length l are both in centimetres. The swimbladder semi-minor axis is calculated from the relationship:

$$a_{ps}(0) = \sqrt{\frac{3V(0)}{4\pi b_{ps}(0)}} \tag{12}$$

Note that $b_{ps}(0)$ and $a_{ps}(0)$ are quantities at the sea surface.

It is well known that the swimbladder volume of herring decreases with depth following Boyle's law (Ona, 1990), and the dimensions of the swimbladder change with depth as follows (Gorska and Ona, 2003):

$$a_{ps}(z) = a_{ps}(0)\left(1+\frac{z}{10}\right)^{-\alpha} \tag{13}$$

$$b_{ps}(z) = b_{ps}(0)\left(1+\frac{z}{10}\right)^{-\beta} \tag{14}$$

where z is the depth in meters. The values of the α and β are rates proposed by Fässler and colleagues (Fässler et al., 2007; Fässler, 2010) as $\alpha = 0.4$, $\beta = 0.2$.

When elasticity is considered, the resonance frequency of a spherical bubble is (Andreeva, 1964; Holliday, 1972) as:

$$f_0 = \frac{1}{2\pi a_{es}} \left(\frac{3\gamma P(z) + 4\mu}{\rho_f} \right)^{\frac{1}{2}} \tag{15}$$

where μ is the real part of the rigidity of fish flesh (*shear modulus*), γ ratio of specific heat for air, a_{es} the equivalent spherical radius and ρ_f fish tissue density.

In the next step, we obtain the coefficient K in Eq. (3) as well as determine the frequency dependence of the damping term δ – defining this parameter for the frequencies much higher and close to resonance. It enables us to extend the resonance scattering model to the non-resonance frequency range.

The coefficient K is equal to one for the conventional resonant scattering model (Love, 1978; Ye, 1997; Scoulding et al., 2015, 2022) but will allow the differential backscattering cross-section, $\sigma_{bs}(\infty, z)$ approach a constant or an asymptotic value consistent with the Kirchoff Approximation for a normal incidence scenario (Eq. 64 in Gaunaurd, 1985):

$$\sigma_{bs}(f, z) = \frac{a_1 a_2}{4} \tag{16}$$

where a_1 and a_2 are the principal radii of curvature at the centre of the first Fresnel zone of the swimbladder. The approximation can be used because as $f \to \infty$ ($f \gg f_{ps}$), we have $a_1, a_2 > \lambda$, with $\lambda = 2\pi/k$ is the wavelength. Moreover, since our applications are always in the far field of the echosounders, the distances of the target from receiver and source, r and R (in Eq. 64, Gaunaurd, 1985), respectively, satisfies $r, R \gg a_1, a_2$. Note that, in our case, i.e., backscattering or monostatic scattering, these two distances are the same.

For a prolate spheroid as described above, the radii a_1 and a_2 can be expressed in terms of its semi-minor and semi-major axes as:

$$a_1 = a_{ps} \quad \text{and} \quad a_2 = b_{ps}^2 / a_{ps} \tag{17}$$

Both of them depend on depth z implicitly.

To determine the constant K at a particular depth z, for $f \to \infty$ ($f \gg f_{ps}$), we set Eq. (3) equal to Eq. (16):

$$\frac{K\zeta^2 a_{es}^2}{1+\frac{K}{\delta^2(\infty)}} = \frac{a_1 a_2}{4} \tag{18}$$

where $\delta^2(\infty)$ denotes the asymptotic values ($f \to \infty$) of the damping term.

Solving the above equation for $\delta^2(\infty)$, we obtain

$$\delta^2(\infty) = \frac{K\frac{a_1 a_2}{4}}{K\zeta^2 a_{es}^2 - \frac{a_1 a_2}{4}} \tag{19}$$

To ensure the $\delta(f)$ is a real function, we set:

$$\delta^2(\infty) \geq 0 \tag{20}$$

or the denominator in Eq. (19) should be a positive value: $K\zeta^2 a_{es}^2 - \frac{a_1 a_2}{4} > 0$. Hence the coefficient K should satisfy the condition:

$$K \geq \frac{a_1 a_2}{4\zeta^2 a_{es}^2} = \frac{a_2}{4\zeta^2 a_1 \varepsilon^{-2/3}} \tag{21}$$

Here Eq. (5) for a_{es}, the formula for prolate spheroid volume and the relationships given in Eq. (17) have been applied.

If we introduce a constant C in Eq. (21):

$$K = \frac{C a_2}{4\zeta^2 a_1 \varepsilon^{-2/3}} \tag{22}$$

with $C > 1$, the condition $\delta^2(\infty) > 0$ will be satisfied i.e. $\delta(\infty)$ is a real number. Substituting Eq. (22) into Eq. (19) leads to

$$\delta^2(\infty) = \frac{\frac{C a_2}{4\zeta^2 a_1 \varepsilon^{-\frac{2}{3}}}}{C-1} = \frac{a_2 \varepsilon^{\frac{2}{3}}}{4\zeta^2 a_1}\left(\frac{C}{C-1}\right) \tag{23}$$

More analysis of the damping factor at the resonance frequency is important for further derivations. In the case of resonance scattering the parameter can be presented in the form of (Love, 1978):

$$\frac{1}{\delta} = \frac{1}{\delta_{rad}} + \frac{1}{\delta_{vis}} + \frac{1}{\delta_{th}} \tag{24}$$

that is, the sum of the reciprocal quantities for radiation (δ_{rad}), viscous (δ_{vis}) and thermal (δ_{th}) damping components. These components are defined as (Eq. 7 in Scoulding et al., 2022):

$$\delta_{rad} = \frac{\rho_f}{\zeta \rho_w k a_{esr}}$$

$$\delta_{vis} = \frac{\pi \rho_f f a_{esr}^2}{\xi} \tag{25}$$

$$\delta_{th} = \frac{2\pi f a_{es}}{3(\gamma-1)}\left(\frac{\rho_a c_{pa}}{\pi f \kappa_a}\right)^{\frac{1}{2}}\left(1+\frac{s}{2\pi^2 \rho_f f^2 a_{es}^3}\right)^{-1}$$

where ρ_w is the density of the water, ρ_a the density of the gas in the swimbladder, s is the surface tension at the fish flesh and swimbladder interface [N m^{-2}], ξ the viscous coefficient [Pa s], κ_a is the thermal conductivity of air [cal m^{-1} s^{-1} °C^{-1}], and c_{pa} is the specific heat at constant pressure for air [cal kg^{-1} °C^{-1}].

The damping term δ at resonance frequency in Eq. (3) is the quality factor Q (Love, 1978; Ye, 1997; Scoulding et al., 2015), which is a constant to characterize the scattering at the resonance frequency.

Our calculations (not shown here) indicate that the radiation damping term $\frac{1}{\delta_{rad}}$ (Eq. (25)) makes the largest contribution to $\frac{1}{\delta}$ (Eq. (24)): several orders of magnitude larger than the thermal term $\frac{1}{\delta_{th}}$ and the viscosity term $\frac{1}{\delta_{vis}}$. By ignoring the difference in material properties between fish flesh and water, at resonance frequency it can be shown that:

$$\delta_{res}^{-1} \approx \delta_{rad}^{-1} = \zeta k_{res} a_{es} \tag{26}$$

Since both damping factors at the resonance frequency (Eq. (26)) and at high frequencies (Eq. (25)), i.e., δ_{res}^2 and $\delta^2(\infty)$ are larger than 0, a transition function can be constructed: $\delta^2(ka_{es}) \equiv T(ka_{es})$ over the range from $ka_{es} = k_{res}a_{es}$ to $ka_{es} \to \infty$, which ensures $T(ka_{es}) > 0$.

We construct the following transition function (a transient response of a passive electric system to a step function, Alexander et al., 2013):

$$\begin{aligned}\delta^2(k a_{es}) &\equiv T(k a_{es}) \\ &= [T(\infty) - T(0)] \\ &\quad \times \left(1 - e^{-(k a_{es} - k_{res} a_{es})}\right) + T(0)\end{aligned} \tag{27}$$

where

$$T(0) = \delta_{res}^2 = (\zeta k_{res} a_{es})^{-2} = \zeta^{-2} k_{res}^{-2} a_1^{-2} \varepsilon^{2/3} \tag{28}$$

and

$$T(\infty) = \delta^2(\infty) \tag{29}$$

with $\delta^2(\infty)$ satisfies the Eq. (23).

After substitution Eqs. (23) and (28) into Eq. (27) it can be shown that:

$$\delta^2(k a_{es}) = \frac{\varepsilon^{\frac{2}{3}}}{\zeta^2 a_1}\left(\frac{a_2}{4}\frac{C}{C-1} - \frac{1}{k_{res}^2 a_1}\right)$$

$$\times \left(1 - e^{-(k a_{es} - k_{res} a_{es})}\right) \quad (30)$$

$$+ \frac{\varepsilon^{\frac{2}{3}}}{\zeta^2 k_{res}^2 a_1^2}$$

The differential backscattering cross-section of swimbladder $\sigma_{bs}(f,z)$ at the normal incidence (Eq. (3)) can be obtained using Eq. (4) for the factor ζ, Eqs. (5)–(9) for equivalent spherical radius, Eqs. (10)–(15) for the resonance frequency of the swimbladder f_{ps}, Eqs. (17) and (22) for the coefficient K, and Eq. (29) for $\delta^2(ka_{es})$.

The question is what value of the coefficient C to choose in the calculations. As mentioned above, the coefficient C is to ensure that the value of $\delta^2(\infty)$ is positive if C is greater than 1. The value $C = 1.1$ will be used to generate all simulation results shown in the next section.

To take into account the dependence of the scattering on the tilt angle of fish at frequencies much higher than resonance frequency, we adopt the directivity function, $D_{ps}(\theta,z)$, given by Medwin and Clay (1998):

$$\sigma_{bs}(\theta,z) = D_{ps}(\theta,z)\sigma_{bs}(f,z) \quad (31)$$

where

$$D_{ps}(\theta,z) = \frac{\sin^2(2k\, b_{ps}(z)\sin(\theta+\Delta\theta))}{[2k b_{ps}(z)\sin(\theta+\Delta\theta)]^2} \quad (32)$$

$$\times \cos(\theta+\Delta\theta)$$

θ is the fish's orientation angle (the same as in Eq. (1)), and $\Delta\theta$ is the inclination angle of the fish's swimbladder axis relative to its body axis. The target strength (TS, in dB), according to MacLennan et al. (2002) is defined as:

$$TS(f,z) = 10\log_{10}(\sigma_{bs}(f,z)) \quad (33)$$

We made sure that the model produced in this way delivered appropriate results by comparing it with existing models, as described in section 2.2.3. The introduced transition function (Eq. (26)) provided that the developed backscattering model results are consistent with solutions of Gaunaurd (1985) (Kirchoff approximation) and of Scoulding et al. (2015, 2022) (resonance scattering model) for both larger and smaller values of the modeling parameters (ka_{es}) respectively.

2.2.3 Model verification

To verify the newly developed model, we compare it with *MB-DCM* developed by Stanton (1988a,b, 1989). We are aware that *MB-DCM*, similarly to the model proposed by us, is an approximate model. Hence, we made a comparison only over the ka_{ps} – range over which *MB-DCM* produces the results close to those of the more accurate *Boundary Element Method* and *Finite Element Method*, based on the publication of Jech et al. (2015). The comparison of three approaches: the *BEM*, *FEM* and *MB-DCM* is presented in Figure 6c of that publication. We evaluate the dimensionless parameter ka_{ps} corresponding to the frequency range presented in the figure. It corresponded to a range of ka_{ps} from 0.5 to 8. The differences between the models do not exceed 0.33 dB for ka_{ps} smaller than 1 ($ka_{ps} \leq 1$) and 0.2 dB for larger ka_{ps}.

In our study, ka_{ps} at 38 kHz, varies from 0.37 (fish of length 12 cm) to 0.81 (fish of length 25 cm). The common part of this ka_{ps} range and the range aforementioned in the previous paragraph is from 0.5 to 0.81 (this ka_{ps} range refers to fish length from 17 cm to 25 cm). Over this range, *BEM* and *FEM* produce results smaller by ca. 0.33 dB than *MB-DCM* (Figure 6c in Jech et al., 2015). This

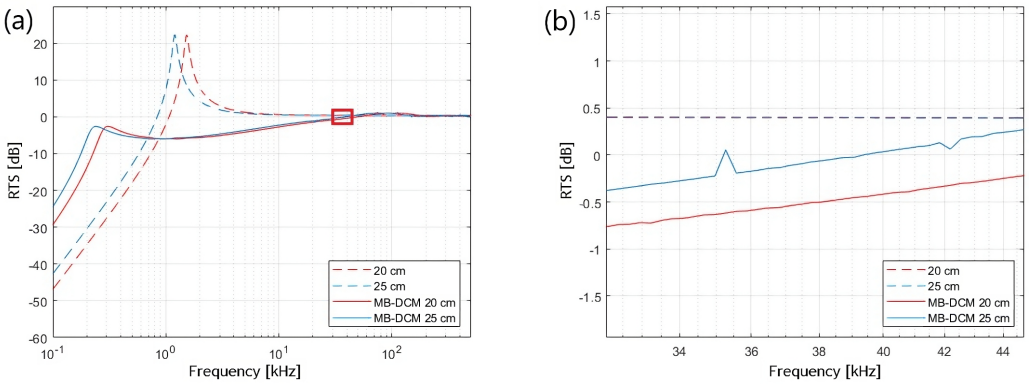

Figure 2. Comparison of our modified resonance model (dashed lines) with the *MB-DCM* (solid lines), for different fish length. Broader range of frequency (a). Zoom-in of the red rectangle in panel (a) around frequency 38 kHz (b), which was the echosounder frequency used in our modelling. In the zoom-in picture, the two dashed lines exactly overlap.

small value suggests that by comparing our results with *MB-DCM* within this ka_{ps} range, we compare them with more accurate *BEM* and *FEM*. Therefore, a comparison between our model and *MB-DCM* enables some of our model verification.

To understand the difference between our model and *BEM* and *FEM*, we should evaluate the difference between our model and *MB-DCM* in the considered ka_{ps} range. Further, working with the parameters: acoustic frequency and fish total length, we control to stay within the considered ka_{ps} range. The *Reduced Target Strength* (*RTS*), defined by the formula: $RTS = TS - 20\log 10(bps/2)$, as a function of acoustic frequency is presented in Figure 2 for different fish lengths (20 and 25 cm – red and blue curves, respectively). The red rectangle in Figure 2a near the frequency 38 kHz indicates the area shown in Figure 2b. The figure demonstrates that *MB-DCM* results achieve lower values than our model results. At a frequency of 38 kHz, used for hydroacoustic herring abundance estimation in the Baltic Sea, the difference is less than 1 dB.

Accounting for that our model predictions will be 1 dB higher than *MB-DCM* (Figure 2b) and that *BEM* and *FEM* give a result lower than *MB-DCM* by ca. 0.33 dB, it can be concluded that the difference between our model and *BEM* and *FEM* could not be higher than ca. 1.33 dB.

2.3 Model input data

All calculations were performed at the acoustic frequency $f = 38$ kHz, which is used for hydroacoustic herring abundance estimation in the Baltic Sea (ICES, 2017). Water density ρ_w was estimated based on an algorithm by Fofonoff and Millard (1983) implemented as an online calculator (Chapman, 2006). Most remaining parameters were directly taken from the literature: the speed of sound in sea water for the southern Baltic c from Grelowska (2000), $\Delta\theta$ from Gorska and Idczak (2021), the ratio of specific heat for air γ from Scoulding et al. (2015). The values of the input model parameters and their sources of references are given in Table 1.

To determine the most appropriate value of the parameter μ, which is included in Eq. (15), the resonance frequency of the swimbladder (Eq. (10)) was calculated for a range of shear modulus (μ) from 10^2 Pa to 10^7 Pa. This is a combined range from two publications: Scoulding et al. (2015) proposed the range from 10^5 Pa to 10^7 Pa, while Fässler (2010) a value of 105 Pa. Then the calculated frequency was compared with the empirical frequency from Simmons and MacLennan (2005). The calculated results are presented in Figure 3, where the dependence of resonance frequency (f_{ps}) on fish total length for different μ values (solid curves of different colours) is shown. These results are compared with the empirical values (black dashed line) taken from Simmonds and MacLennan (2005). The figure shows that the curve closest to the empirical one is obtained at the value of $\mu = 10^6$ Pa (violet curve, Figure 3). Therefore, in the following calculations, we used value $\mu = 10^6$ Pa.

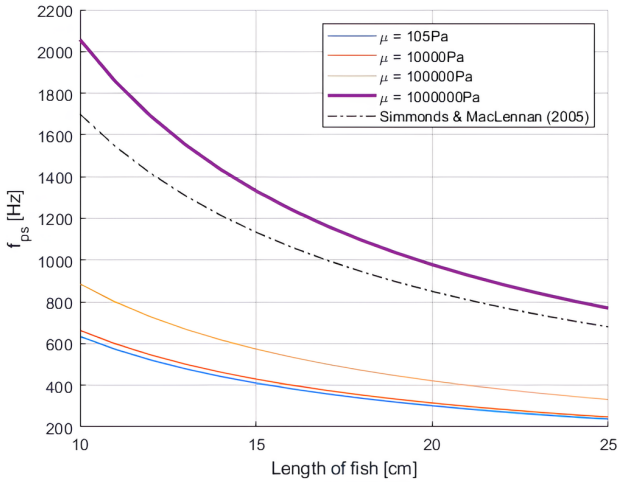

Figure 3. Dependence of resonance frequencies on fish total length for different values of parameter μ, compared with the empirical curve from Simmonds and MacLennan (2005) (dotted line).

From the literature, two values of volume percentages

Table 1. Parameter values used to estimate the target strength of the herring.

	Symbol	Unit	Value used in the model	References
Frequency	f	Hz	38000	Grygiel et al. (2011)
Sound speed in sea water	c_w	m s^{-1}	1450	Grelowska (2000)
Density of sea water	ρ_w	kg m^{-3}	1006	Fofonoff and Millard (1983)
Density of fish flesh	ρ_f	kg m^{-3}	1071	
Offset of the swimbladder axis relative to the body axis	$\Delta\theta$	[°]	3.2	Gorska and Idczak (2021)
Ratio of specific heat for air (swimbladders)	γ	–	1.4	Scoulding et al. (2015)
Shear modulus	μ	Pa	10^6	Sensitivity analysis
Constant providing real value of $\delta(\infty)$	C	–	1.1	By fitting to the exact MSS for a spherical bubble

of swimbladder relative to the total fish volume, n, were reported: 5% (Ona, 1990) and 15% (Nero et al., 2004). The first volume percentage, i.e., $n = 0.05$, was used in the later model calculations since it provided a better fit to the measured TS histograms for the Baltic herring.

The parameters in the fish weight-length linear regression formula (the scaling factor and the power factor) were taken from Kasatkina (2007, Table 1: *Fish weight–length regression based on data 2002–2005*; data for adult herring, fall season).

2.4 Collection and analysis of hydroacoustic and biological data

Data collection

The hydroacoustic and fish data were collected on board the r/v *Baltica* inside the Polish Exclusive Economic Zone during a hydroacoustic survey in September/October 2010. The cruise was related to the Polish component of the BIAS (Grygiel et al., 2011).

The vessel was equipped with a Simrad EK60 echosounder with a split-beam, hull-mounted, downward-facing, 38 kHz transducer (Table 2). Prior to the survey, the echosounder system was calibrated following the standard procedures (ICES, 2017) using a standard 60 mm diameter copper sphere as recommended by the manufacturer.

Table 2. Transducer characteristics and Simrad EK60 echosounder settings during single-target data collection.

Parameter	Value
Transducer type	ES38-B
Transmitting power	2000 W
Pulse duration	1.024 m s
Ping rate	1 s^{-1}
Beam width	7°
Two-way beam angle	−20.6 dB

The echosounder was running continuously during the survey so that the hydroacoustic data were available for each trawl station. Complete trawl information is presented in Appendix B for all hauls selected for the analysis.

Data analysis

To determine the acoustic target strength, hydroacoustic data were processed using SonarData Echoview software (Echoview 4.90.81.19054). The analyzed layer was the same as the trawled layer. The parameters used for the single target detection algorithm were: minimum TS value: −80 dB; minimum and maximum echo length ratio: 0.7 and 1.3; maximum beam compensation: 6 dB; maximum standard deviation of axis angle: 0.6 deg. Finally, single target detections from fish were filtered to exclude all targets > 3° off the transducer beam axis. For all remaining single target detections the parameters as TS and depth were obtained and used in further analysis.

Analysis of fish species composition of trawls enabled the selection of trawls for the processing of hydroacoustic data. We considered only the hauls in which herring comprised > 90% of catch by number. For the analysis, we choose four hauls satisfying this condition. For each of these hauls, we also calculated a Sawada Index to ensure that we had a high proportion of single targets. The Sawada Index is a parameter to quantify the percentage of multiple echoes in the received signal (Sawada et al., 1993), to evaluate the quality of the collected hydroacoustic data. Different authors provide different values of this index to make the TS measurement reliable (e.g. < 0.04, < 0.1). We were based on Peltonen and Balk (2005), who only took into account hauls with acoustic recording where the index values were < 0.2.

The number of detected single echoes, the average TS, and the Sawada Index, which are important to understand the accuracy of the in situ TS measurements, are presented in Table 3 for four selected hauls.

Table 3. Number of echoes, average TS, and the Sawada Index of echoes detected in acoustic measurements coresponding to choosen hauls.

Haul no.	Number of detected single echoes	Average TS (based on catch results)	Sawada Index
7	1457	−46.17 dB	0.17
25	1027	−45.05 dB	0.14
26	593	−45.25 dB	0.10
27	137	−45.19 dB	0.06

To develop the algorithm for estimation of individual herring orientation, described in the next subsection, the measured TS distributions for the selected hauls were cut off at the −34 dB threshold, because TS values above this value were highly unlikely coming from individual Baltic herring (Fässler and Gorska, 2008, 2009). Moreover, a lower cut-off threshold was also applied to the measured TS data. Two lower cut-off thresholds were selected for comparison: −60 dB and −55 dB. They correspond to the lower limit of Baltic herring TS, as shown by a number of measurements (Lassen and Staehr, 1985; Didrikas and Hansson, 2004; Peltonen and Balk, 2005, Schmidt et al., 2011), as well as by theoretical calculations (Gorska, 2007; Fässler et al., 2007, 2008; Fässler and Gorska, 2009; Gorska and Idczak, 2021). In the cited experimental studies, it was assumed that TS lower than the selected thresholds were likely from other targets smaller than Baltic herring individuals.

In addition to fish species composition for each haul, fish total length distribution was determined (Figure A1). Using the hydroacoustic data collected for each haul, the depth distribution of single echoes (as described above) was obtained (Figure A2).

2.5 Algorithm for estimation of individual herring orientation

To develop the algorithm for each haul selected for analysis, the following procedures were applied:

1. First, herring TS histograms were calculated using the scattering model described in section 2.2 and the input parameters presented in section 2.3 for a series of numerically generated fish aggregations with a normal distribution of orientation angles of individuals, i.e., Eq. (1). The herring total length distribution was taken for the selected haul. The fish distribution over the depth was obtained from the echogram corresponding to this haul. In the calculations, the mean angle $\overline{\theta}$ was changed over the range from 0° to −50° with a 2.5° increment, while the standard deviation s_θ – over the range from 4° to 40° with a step of 2°. Negative theta angles were used on the assumption that fish were more likely to run away from a noisy ship than to swim toward it. Apart from that, the issue is almost symmetrical – only the offset of the swim bladder position causes a bias in one direction.

   In Figure 4 this step is presented by the top left rectangle divided into smaller rectangles. Each of these small rectangles involves the TS-histogram computed at values of mean angle $\overline{\theta}$ and the standard deviation s_θ from the mentioned ranges. This large rectangular symbolizes the "matrix" of TS histograms as presented in Figure 6.

2. Then, for the selected haul, each TS histogram, generated over the entire considered range of $\overline{\theta}$ and s_θ, was compared with the measured TS histogram, using the χ^2 (chi-square) test. The χ^2 distance was used as a measure of similarity between the two histograms (Pele and Werman, 2010) and is defined as:

$$\chi^2 = \frac{1}{2}\sum_{i=1}^{n}\frac{(x_i - y_i)^2}{(x_i + y_i)} \tag{34}$$

   where n is the number of bins in each of the measured and theoretical TS histograms, and x_i and y_i are the TS values of the ith bin of the theoretical and measured TS distributions, respectively.

   The difference between the measured TS distribution and the theoretically predicted TS distribution calculated for each chosen pair of $\overline{\theta}$ and s_θ was then assigned to a corresponding χ^2 distance. These values, calculated over the entire considered range of $\overline{\theta}$ and s_θ, form χ^2 distance matrix. In Figure 4 each of the small rectangles, included in the top large rectangle, can be assigned to the χ^2 distance, calculated for the $\overline{\theta}$ and s_θ corresponding to this small rectangle. It means that the larger rectangle symbolizes also the matrix of χ^2 distances.

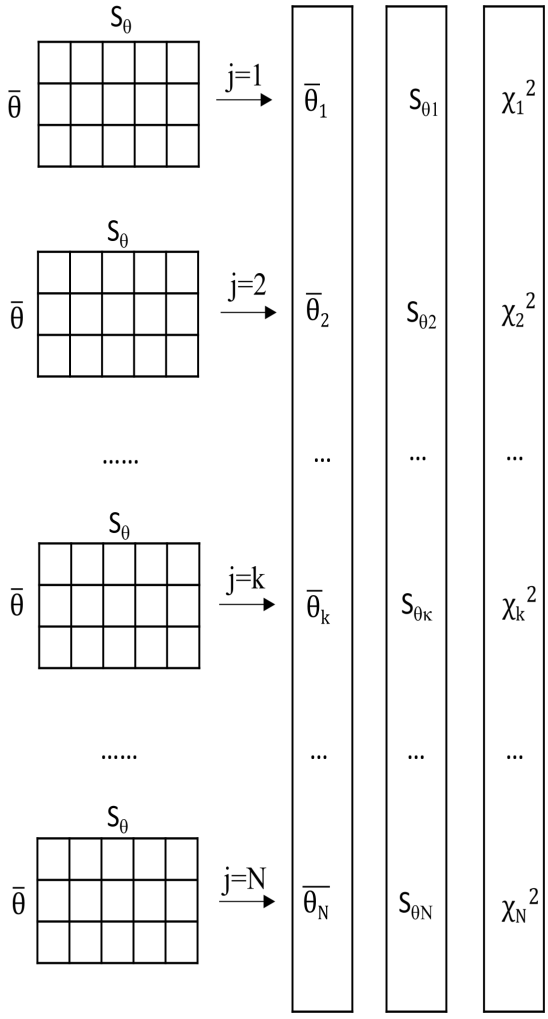

Figure 4. Schematic representation of the algorithm. The $\overline{\theta}$, s_θ and χ^2 values are calculated for each repetition.

The smaller the χ^2 distance, the more likely that the corresponding orientation distribution of herring individuals represents the actual orientation distribution of herring aggregation during the measurements. Consequently, the parameters ($\overline{\theta}$ and s_θ) corresponding to the minimum element of the described χ^2 distance matrix, would be considered as the best estimated parameters of the actual distribution. In Figure 4 the parameters ($\overline{\theta}$ and s_θ) corresponding to the minimum element of the described χ^2 distance matrix are presented right side from the top rectan-

gle: $\overline{\theta}_1$, $s_{\theta 1}$ while the minimum χ^2 as χ^2_1.

3. For each haul the procedure described in points 1 and 2 above, was applied N-times (N realizations, see N-levels in Figure 4). This approach is to achieve more robust estimates, as well as to assess the variability or uncertainty of the estimates. At each step j ($j = 1 : N$) the $\overline{\theta}_j$ and $s_{\theta j}$, (from Eq. (1)), for which the fit of the numerically calculated and measured TS – histograms was the best, as well as the χ^2_j (χ^2 distance) were determined, as it was presented above in points 1 and 2. As a result, the three data series of the parameters $\overline{\theta}_j$ and $s_{\theta j}$ and χ^2_j ($j = 1 : N$) were obtained. In Figure 4 these series are shown by vertically elongated rectangles. For the two first data series mean values ($\langle\overline{\theta}\rangle$ and $\langle s_\theta\rangle$) were calculated. Additionally, associated standard deviations SD1 and SD2, characterizing respectively the variability of the mean angle $\overline{\theta}_j$ – and the associated standard deviation $s_{\theta j}$, were also computed. We used $N = 100$.

3. Results and discussion

Before applying the developed hydroacoustic techniques for determining the orientation distribution of the aggregated Baltic herring, herring backscattering properties, which are required for algorithm development, are analyzed in sections 3.1 and 3.2.

3.1 Herring backscattering properties: the directivity function

The newly developed model presented here not only became the basis of the developed algorithm to infer herring orientation distribution but also allowed a new look at some of the herring backscattering properties.

Using the developed scattering model (section 2.2) with the input data (section 2.3), the dependence of herring TS on their orientation angle (θ) was estimated based on their measured total lengths ranging from 10 to 25 cm and at an exemplary depth of $z =$ m. The backscattering directivity functions are shown in Figure 5. The functions are symmetrical in relation to its maximum, which occurs when the longitudinal axis of the swimbladder is perpendicular to the incident wave. Since the swimbladder is not aligned with the fish body, the maximum function value will not occur at the angle $\theta = 0°$ but shifted by an angle of $\Delta\theta$, which is the offset of the swimbladder lengthwise axis relative to the body lengthwise axis.

The positions and number of minima (nulls) of the directivity function change depending on the fish length (Figure 5). The directivity function for 10 cm fish (blue line) has two minima, while for the larger fish (15 and 20 cm, orange and red lines, respectively), the functions have additional third minimum.

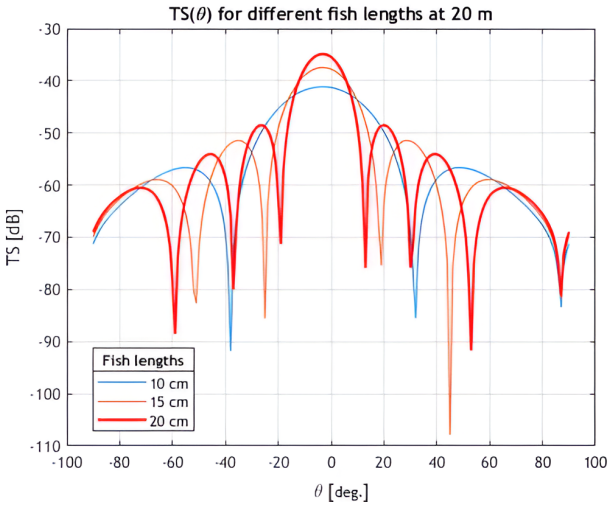

Figure 5. Directivity functions (dependence of TS on orientation angle θ) at 38 kHz for fish of various total lengths. The bold red line shows the TS curve for the fish total length $l = 20$ cm.

3.2 Herring backscattering properties: the modality of the TS distributions

TS histograms were calculated using Gaussian PDF for the mean ($\overline{\theta}$) and standard deviation (s_θ) angles (Eq. (1)) varying over the intervals of 0° to 50° and 4° to 40°, respectively. A set of TS distributions corresponding to these pair of orientation parameters is presented in Figure 6. The shape of TS distributions changes with $\overline{\theta}$ and s_θ. It is observed that for each $\overline{\theta}$ an increase in s_θ can result in a bimodal or even a trimodal TS distribution.

For small values of the standard deviation s_θ, the TS distribution remains unimodal, even for larger mean orientation angle $\overline{\theta}$. This is shown in Figure 6, where with the standard deviation $s_\theta = 4°$ (first column of the table) for the entire range of mean angle $\overline{\theta}$ from 0° to 50°, unimodal distributions on TS histograms are observed.

On the histograms for a small $\overline{\theta}$ ($\overline{\theta}$ equal to 0°, e.g., top row in Figure 6), to the left of the main peak (primary mode), i.e., for lower TS values, a second peak (second mode) with lower amplitude (lower occurrence frequency of TS values) appears with an increased s_θ. The first sign of the formation of a bimodal TS distribution appears at a standard deviation of about 12°. With an increasing standard deviation, the division into two modes becomes more pronounced (for s_θ 20° and 28°). The position of the peak of the primary mode does not change much over the entire range of s_θ. The primary mode is the mode corresponding to the smallest s_θ (i.e., the first column of Figure 6) and is persistent in the entire range of s_θ.

For two modes to arise in TS – histogram, the standard deviation of orientation distribution must be large enough to include two lobes from the backscattering directivity

function of individual fish (Figure 5). For example, for a fish total length of 20 cm, Figure 5 shows the minima of the directivity function at 13 and 30 degrees. Hence, it can be expected that for an unimodal fish orientation distribution containing these minima in the orientation range, the herring TS distribution does not have to be unimodal. It explains, for example, well visible two-mode TS – histograms for $\overline{\theta} = 10°$ in the range from $s_\theta = 12°$ to $s_\theta = 28°$.

3.3 Algorithm of inferring herring individual orientation

3.3.1 The impact of acoustic data processing on results of the algorithm application

The effect of applying a lower cut-off TS threshold to the measured data on the results of the developed algorithm (section 2.5) was investigated for the selected hauls. The sensitivity analysis of the obtained orientation distribution to the lower cut-off TS threshold was also carried out. The results of sensitivity analysis for haul z7, as well as some chosen statistics of the $\overline{\theta}$ and s_θ, estimated using the algorithm described in section 2.5, for all selected hauls are presented in this subsection. The detailed results for hauls z25, z26, z27 are included in Appendix A.

The sensitivity analysis for haul z7

The values of $\langle\overline{\theta}\rangle$ and $\langle s_\theta\rangle$ with standard deviations SD1 and SD2 (see section 2.5) for haul z7 are presented in Table 4 for the two lower cut-off TS thresholds. The comparison demonstrates lower absolute values of $\langle\overline{\theta}\rangle$ and lower $\langle s_\theta\rangle$ for a higher threshold value of -55 dB. This means a smaller mean orientation angle deviation from 0 and a tighter spread of orientation angle (an indication of a more synchronized movement of aggregated fish).

Table 4. Impact of lower cut-off TS threshold on mean orientation angle and the standard deviation.

Lower TS threshold applied to the measured data	-60 dB	-55 dB
$\langle\overline{\theta}\rangle \pm$ SD1 [°]	-19.9 ± 0.66	-15.4 ± 0.92
$\langle s_\theta\rangle \pm$ SD2 [°]	9.93 ± 1.5	6.02 ± 0.31

A 2D colour visualization of the χ^2 distance matrix described in subsection 2.6 is presented in Figure 7a and b for the two lower cut-off TS thresholds, -60 dB and -55 dB, respectively. As it was described in point 3 of subsection 2.5 for each haul the three data series of the parameters $\overline{\theta}_j$ and $s_{\theta j}$ and χ^2_j $(j = 1 : 100)$ were obtained. Then the minimum of the data series $\{\chi^2_j\}$ $(j = 1 : N)$ was indicated.

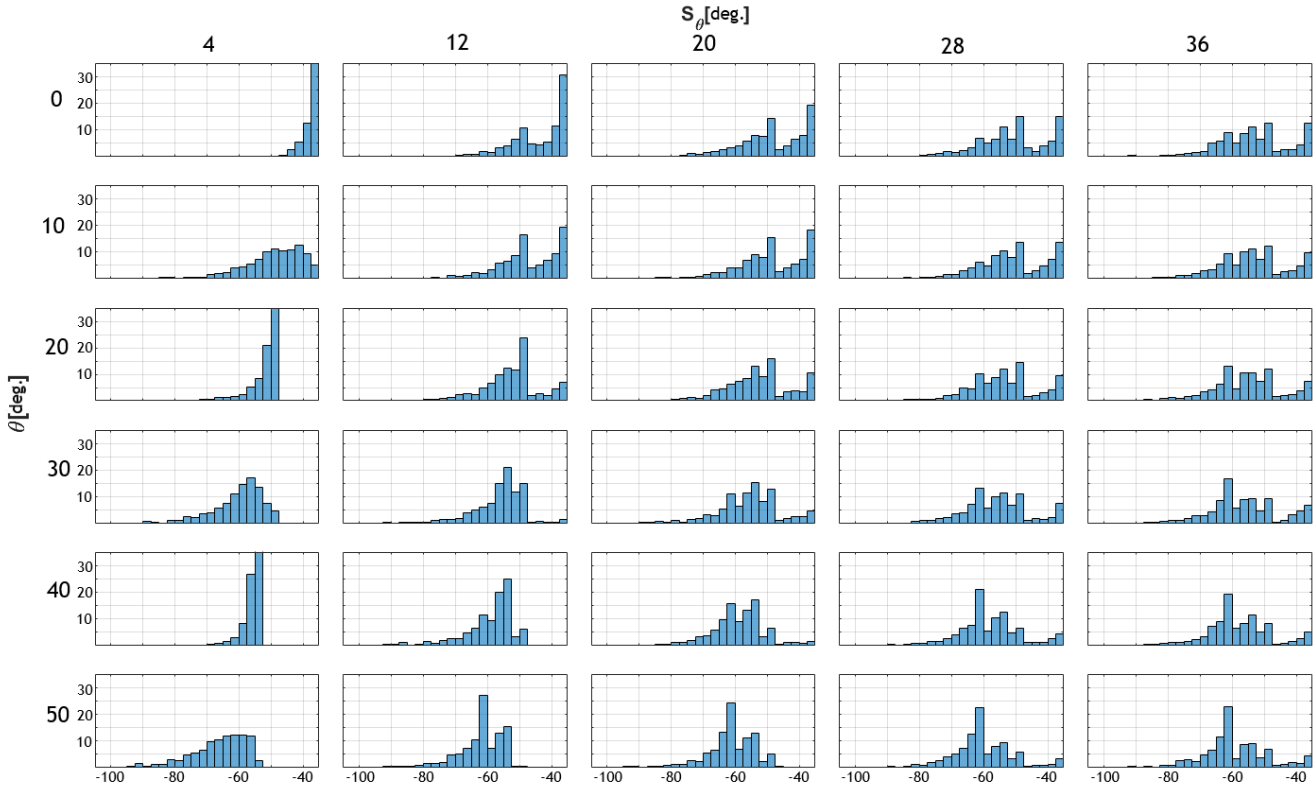

Figure 6. TS table of histograms for different distributions over fish orientation, for herring individual of 20 cm long, at a depth of 20 m. The mean orientation in the range of 0°–50° changing with 5° steps, is presented on the vertical axis while the standard deviation s_θ changing from 4° to 28° in 8° steps is presented in horizontal axis.

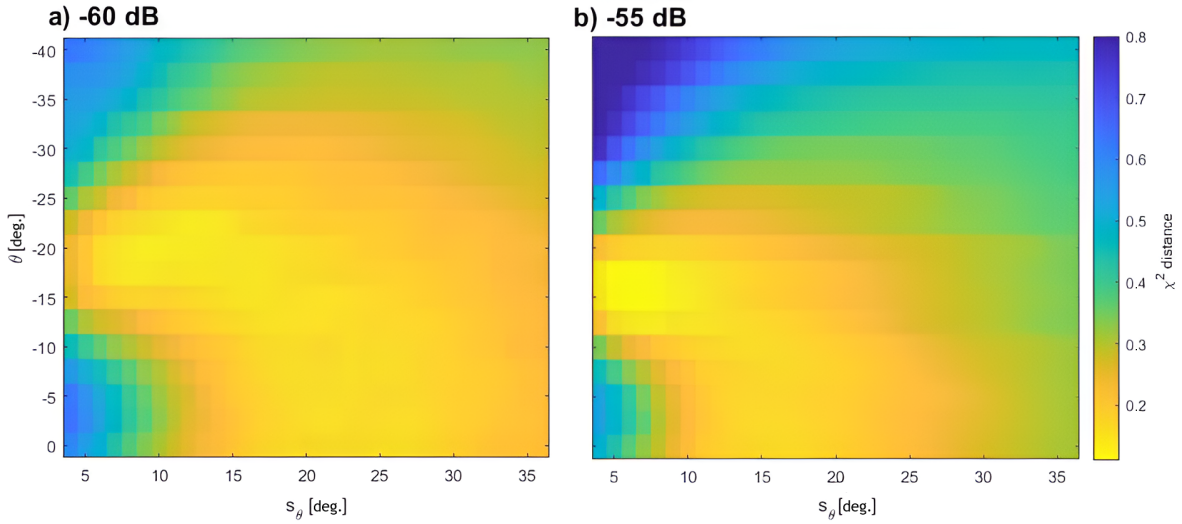

Figure 7. Colour maps of the χ^2 distances between the modeled TS distributions and the distribution measured in hauls z7 for two lower cut-off TS thresholds: -60 dB (a), -55 dB (b).

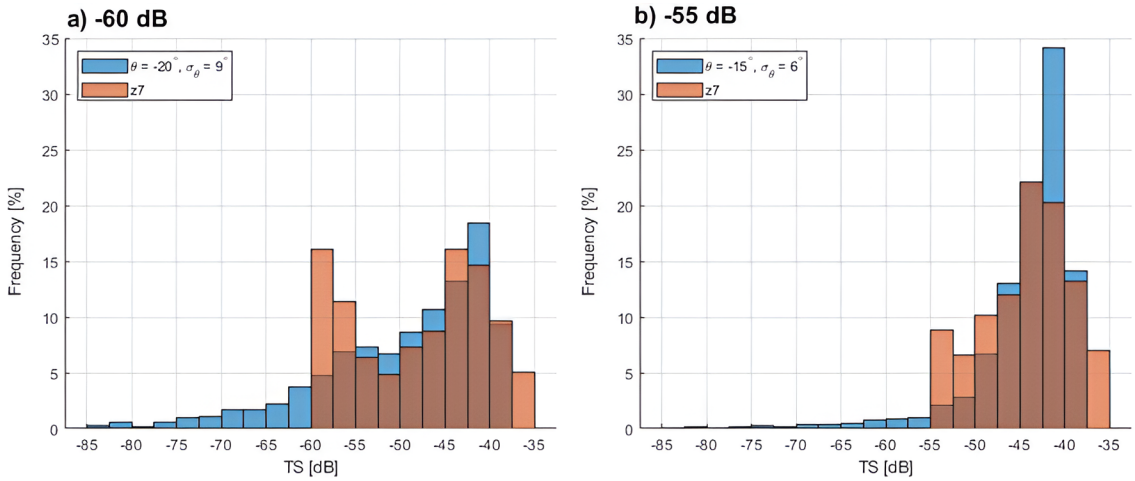

Figure 8. Comparison of histograms fit for two thresholds – distribution of TS measured in the z7 haul (orange) and the closest theoretical distribution (blue).

Let it be for $j = k$ in Figure 4. Figures 7 and 8 demonstrate the calculation results corresponding to the realization $j = k$.

In Figure 7, panels a and b, the colour scale corresponds to the value of the χ^2 distance: darker blue colour corresponds to a worse fit (higher values of the χ^2 distance) between the simulated or theoretically predicted and measured TS distributions. A 2D colour map of the χ^2 distance matrix provides a good visual representation to easily identify the ranges of $\overline{\theta}$ and s_θ that provide good and bad fits. In addition, local minima and maxima are also easily identifiable. From Figure 7, it can be observed that the gradient of the χ^2 distance function is much steeper for the -55 dB threshold. The minimum of the χ^2 distance for this threshold occurs for a smaller standard deviation of the orientation distribution, and slightly smaller mean orientation angle $\overline{\theta}$. However, both plots show a similar overall pattern, an indication of the robustness of our orientation estimation.

In Figure 8 the numerical TS histograms corresponding to the smallest χ^2 distance (i.e. for χ^2_k in Figure 4), marked by blue colour bars, were compared with the measured TS histogram (orange colour bars). For this χ^2 distance $\overline{\theta} = -20°$, $s_\theta = 9°$ for -60 dB and $\overline{\theta} = -15°$, $s_\theta = 6°$ for -55 dB. A cutoff at the -55 dB threshold results in an unimodal measured TS histogram (Figure 8b). However, for the -60 dB threshold remnants of an additional, lower TS mode remain. It may indicate some objects other than Baltic herring such as some mesopelagic fish, whose TS values are less than -55 dB but greater than -60 dB, might present but not caught by the trawl. The numerically generated TS histogram, obtained for a single species, is

unimodal and hence better fits the measured histogram for the −55 dB threshold than for the −60 dB threshold.

Statistics of the $\overline{\theta}$ and s_θ, for all selected hauls

To obtain results that provide more quantitative information on the comparison between the measured and simulated data, the algorithm was implemented multiple times according to the procedure described in section 2.5. The sets of parameters $\overline{\theta}$ and s_θ obtained from 100 implementations of the algorithm for four selected hauls listed in Table 3 are presented in the form of boxplots in Figure 9a and b respectively. Results using the data with −60 dB lower cutoff threshold are shown in blue while those with the −55 dB threshold are in red.

The series of the parameter χ^2 distances between measured and best-fitted modelled TS histograms obtained for 100 implementations of the algorithm are presented in a similar way in Figure 9c for the four considered hauls.

Figure 9a and b demonstrates that for hauls z7 and z27, both series of $\overline{\theta}$ and s_θ had narrower variabilities than for the other two hauls for both thresholds, indicating that for these two hauls aggregated fish swim more synchronized than in case of hauls z25 and z26. For the haul z7 as well as haul z26, an increase of the TS threshold resulted in a decrease of the absolute value of the mean $\overline{\theta}$ (angle changed towards zero). This is because larger absolute value of the mean $\overline{\theta}$ could be responsible for smaller TS values accounted in case of "−60 dB" threshold.

Conversely, Figure 9b and c shows that for all hauls except for z27 a higher TS threshold of −55 dB leads to smaller parameters s_θ and χ^2 than those obtained using a lower TS threshold of −60 dB.

Figure 9c presents that for haul z26 the fit between measured and modelling TS histograms is the worst, especially for the lower TS threshold of −60 dB (χ^2 distance around 0.21). The smallest χ^2 distance is for haul z7, with the TS threshold of −55 dB (χ^2 distance around 0.1).

The reason for this smaller χ^2 distance for the larger threshold for the haul z7 has been above (discussion concerning Figure 8). As it was shown for haul 7, the use of a higher TS threshold (−55 dB) results in removing the second TS mode in the measured TS data. It could result in a better fit (smaller χ^2 distance) in the case of unimodal numerically obtained TS histograms. Such a result happens not only to haul z7 but also to haul z25 (see Figure A3 in Appendix A).

In the case of the data with two modes (haul z26), the calculated TS histogram with the higher TS threshold can also reduce the χ^2 distance (see Figure A3 in Appendix A). However, the case for haul z27 is an exception, where no clearly visible modal structure in the measured TS histograms (see Figure A3 in Appendix A). The increase of the TS threshold can result in the increase of χ^2 distance.

A large spread of χ^2 distance could suggest that it would not be possible to approximate the orientation distribution

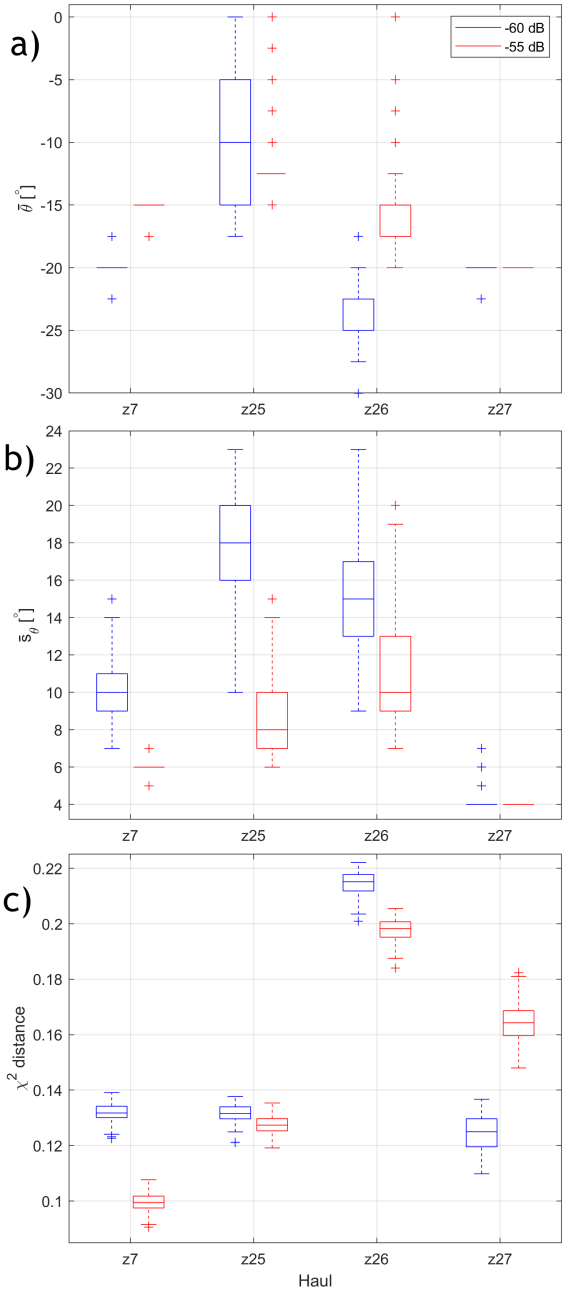

Figure 9. Boxplot of inferred mean orientation ($\overline{\theta}$) values for hauls z7, z25, z26 and z27 from 100 realizations (a). Boxplot of inferred angle standard deviation (s_θ) values for hauls z7, z25, z26 and z27 from 100 realizations (b). Boxplot of the shortest χ^2 distances between the modeled TS distributions and the distribution measured for hauls z7, z25, z26 and z27, from 100 realizations (c).

On each box, the central mark indicates the median and the bottom and top edges indicate the 25th and 75th percentiles, respectively. For some of them, their 25th and 75th percentiles overlap with the median. In panel (a) in case of the haul z26 the median overlap with the upper border of the box. The whiskers extend to the most extreme data points, not including outliers. The outliers are presented individually using the '+' marker.

Table 5. Synthetic comparison of herring orientation angles measured in various experiments.

Reference	$\overline{\theta}$	s_θ	Remarks
Mitson and Knudsen (2003)	−12°	–	while fleeing from the passing vessel, value estimated from school depth measurements
Hjellvik et al. (2008)	−19°	–	while fleeing from the passing vessel, value estimated from school depth measurements
Olsen et. al. (1983)	−27.5°	5.0°	while fleeing from the passing vessel
Ona (1984)	−3.9°	12.8°	for 1819 individuals of herring at a depth of 1.5 m
	0.2°	11.9°	for 898 individuals of herring at a depth of 4 m
	8.1°	16.9°	for 874 individuals of herring at a depth of 30 m
Ona (2001)	−1.1°	10°	for a single adult herring observed for 30 hours in a pen close to the surface
	−3.1°	14.2°	for 943 herring individuals in the pen at depths up to 30 m
Huse and Ona (1996)	0°	10°	for aggregation of herring at night at 62 m
	−10°	5°	for aggregation of herring at day at 200–260 m
	40°	10°	for aggregation of herring at night, at depths of 330–360 m
	30°, −30°	–	bimodal distribution with both positive and negative modes, daytime at depths of 330–360 m

with an unimodal normal distribution – the use of more complex, multimodal approximations could be the next step for further development of the algorithm.

3.3.2 Inferred fish orientations – possible interpretation

Figure 9a and b demonstrates that most orientation angles obtained using the proposed method are quite steep (−17.5°–−25°). This may be related to the reaction of fish to vessel noise (Olsen et al., 1983; Mitson, 1995; Vabø et al., 2002; Mitson and Knudsen, 2003; Simmonds and MacLennan, 2005; Hjellvik et al., 2008). The results presented in the cited publication are discussed below. It is demonstrated that they are in accordance with our results that were obtained when vessel avoidance action could occur, which could explain the obtained angle values in the range up to −25° (Figure 9a).

Based on Figure 6 in Mitson and Knudsen (2003), the orientation of herring when escaping from the vessel (noise) can be estimated. Echogram presented in Figure 6 in that paper allows us to estimate the average diving speed of the herring into the deep. The herring dipped approximately 12 meters per minute, or according to the vertical component of the velocity vector approximately 0.2 m s^{-1}. Assuming that the maximum speed of the herring is about 1 m s^{-1} (Boyar, 1961), it can be calculated that the minimum possible orientation angle of the herring escape into the depths was about −12°. It could be much larger if the herring was swimming slower than the reported maximum swimming speed of Baltic herring.

Performing analogous calculations based on Figure 2 of Hjellvik et al. (2008), which showed some example echograms from the echosounder when a vessel passed by, the minimum possible value of the orientation angle was approximately −19°. These angle values, presented in Table 5, are within the range of our results. Orientation measurements of herring individuals observed at a depth of 40–50 m during their response to a passing vessel by Olsen et al. (1983), resulted in a mean orientation angle of −27.5° with a standard deviation of 5.0°. In this case, it is also in accordance with our results. In comparison, angles measured under conditions where the herring are not disturbed by vessel noise – in isolated pen experiments (Ona, 1984, 2001) or significant depth (Huse and Ona, 1996), are much less steep than those discussed above, measured when the vessel avoidance reaction occurs (Table 5). Steep angles $\overline{\theta}$ of about 30° or 40° (Huse and Ona, 1996) occurred even at very great depths (more than 330 m). It was due to the herring's adjustment to negative buoyancy at the large depth when the swimbladder is highly compressed by hydrostatic pressure.

Because of the significant impact of fish orientation on their TS, the vessel avoidance reaction means that previously accepted Baltic herring hydroacoustic abundance estimations, which has used the *TS-length* regression, recommended by ICES (ICES, 2017), might have produced biased results if the dependence of TS on orientation had not been correctly accounted for (Olsen et al., 1983; Mitson, 1995; Vabø et al., 2002; Simmonds and MacLennan, 2005, Hjellvik et al., 2008). Hence more emphasis should be placed on fish orientation measurements.

3.3.3 The influence of the species composition of the haul on the performance of the algorithm

The algorithm for determining the orientation of aggregated fish has been developed for adult Baltic herring. During BIAS cruises dedicated to measuring herring abundance, on average every fourth haul contains more than 80% of herring. To determine the orientation of herring observed by the vessel's echosounder just before such a haul, the developed method can be applied directly.

The remaining hauls are purely sprat hauls (more than 80% sprat) or mixed hauls (herring plus sprat, the percentage of other species is negligible). The hauls of the first type constitute on average about one-third of all hauls. On the other hand, during the Baltic Acoustic Spring Survey (BASS) cruises, dedicated to Baltic sprat abundance estima-

tion, the percentage of purely sprat hauls is close to 100% (on average about 95%). The question arises whether the developed method can also be used for sprat hauls.

As discussed in subsection 2.2.1, the backscattering of herring individuals takes place in the transition region between the Rayleigh and Kirchoff scattering modes and in the Kirchhoff mode for larger herring individuals. Analyzing Figure 1a, we can conclude that for Baltic sprat, the total length of which varies from about 7 cm to about 14 cm, the parameter kb_{ps} is less than 3, while the parameters ka_{es} and ka_{ps} are less than 1. It seems that for sprat we also have a transitional backscattering mode, which suggests that both, the developed model and the algorithm, can be used also for sprat, but with some reservations. These reservations concern, the morphometric ratios (Eq. (11)) and the relationship between the weight of the individual and its total length (Eq. (9)). They are derived for adult herring (Kasatkina, 2007; Gorska and Idczak, 2021). For sprat, the results of studies on the biological characteristics of sprat (Kasatkina, 2007; Fässler and Gorska, 2009) should be used. It is also necessary to verify the input data to the model presented in subsection 2.3.

That is, by summing up BIAS to over half of the hauls (in the average), we can use the developed method to determine the tilt angle distribution of fish. On the other hand, during BASS-type cruises, we can use the developed algorithm for almost all hauls, modifying it as mentioned above.

We think that by applying the developed algorithm to purely herring (or purely sprat) hauls, we will obtain information about the orientation of the collected fish. This will provide us with a foundation for future research on correcting the relationship between the fish target strength and its length introducing fish orientation. Using these more accurate TS values will increase the accuracy of estimating fish stocks, which will improve resource management.

4. Conclusions

In this paper, a modified backscattering model with a relatively simple analytical form is proposed to describe the acoustic backscattering by herring swimbladder, which is approximated by a prolate spheroid. Although it is an approximate model, it functions almost exactly the same as the resonance scattering model below and around the resonance frequency of fish swimbladder and can also predict the swimbladder backscattering at higher frequencies. This newly developed model is the basis for a more reliable algorithm to estimate herring orientation in the case of transition region mode of backscattering.

In addition, the understanding of the backscattering by Baltic herring has been improved. The obtained results indicate that contrary to the existing view, even a unimodal distribution of fish spatial orientation can cause a bimodal shape of the fish TS distribution. Until now, it was believed that a bimodal TS distribution can only result from a bimodal distribution of one of the key parameters for calculating TS, such as the orientation or size of the fish.

The method proposed in this article allows the estimation of the statistical distributions of the orientation of herring individuals (mean orientation and standard deviation) based on a comparison of the modelled and measured histograms of the TS in the aggregation. The proposed method requires a priori knowledge of fish length distribution and species composition in the observed aggregations. The results from applying this method shown in this paper are promising, where the orientation distributions of herring for four in situ scenarios have been inferred. It has been demonstrated that, in all cases, the escape of herring from the vessel (diving reaction) was highly probable. Due to the strong dependence of the TS on fish orientation, it is recommended to introduce the orientation dependence in the *TS-length* relationship used in hydroacoustic herring abundance estimation in the Baltic Sea.

The technique to determine fish orientation distribution is crucial for more accurate fish abundance estimation. The technique, developed here for Baltic herring, will be the basis to introduce the orientation dependence in the relationship between the fish target strength and its total length. The use of information about the orientation of herring individuals in aggregations can allow for more accurate abundance estimation and enable a more accurate interpretation of the hydroacoustic data collected for Baltic herring stocks. The developed backscattering model and the developed algorithm can also be applied to determine spatial orientation of Baltic sprat. Contrary to the previously developed methods inferring fish orientation distribution, the developed method also allows extracting fish orientation information from the data collected in routine cruises, without the need for additional, complicated and expensive equipment.

Acknowledgement

The data used in this paper were collected by the National Marine Fisheries Research Institute in Gdynia (r/v *Baltica*) in the frame of the Polish component of the BIAS surveys under the EU Data Collection Framework (CDF).

Conflict of interest

None declared.

Supplementary materials

Please follow this link to see the supplementary material associated with this article.

References

Alexander, C.K., 2013. *Fundamentals of electric circuits*. McGraw-Hill.

Andreeva, I.B., 1964. *Scattering of sound by air bladders of fish in deep sound-scattering ocean layers*. Sov. Phys. Acoust. 10, 17–20.

Beltestad, A.K. 1973. *Feeding behavior and vertical migration in 0-group herring (Clupea harengus) in relation to light intensity*. Cand. Real. thesis, Univ. Bergen (in Norwegian).

Blaxter, J.H.S., Batty, R.S., 1990. *Swimbladder "behaviour" and target strength*. Rap. Proces. 189, 233–244.

Blaxter, J.H.S., Hunter, J.R., 1982. *The biology of the clupeoid fishes*. Adv. Mar. Biol. 20, 1–223. https://doi.org/10.1016/S0065-2881(08)60140-6

Boyar, H.C., 1961. *Swimming Speed of Immature Atlantic Herring with Reference to the Passamaquoddy Tidal Project*. T. Am. Fish. Soc. 90, 21–26. https://doi.org/10.1577/1548-8659(1961)90[21:SSOIAH]2.0.CO;2

Burwen, D., Nealson, P., Fleischman, S., Mulligan, T., Horne J., 2007. *The complexity of narrowband echo envelopes as a function of side-aspect angle*. ICES J. Mar. Sci. 64, 1066–1074. https://doi.org/10.1093/icesjms/fsm074

Cardinale, M., Arrhenius, F., 2000. *Decreasing weight-at-age of Atlantic herring (Clupea harengus) from the Baltic Sea between 1986 and 1996: a statistical analysis*. ICES J. Mar. Sci. 57, 882–893. https://doi.org/10.1139/f00-221

Casini, M., Kornilovs, G., Cardinale, M., Möllmann, C., Grygiel, W., Jonsson, P., Raid, T., Flinkman, J., Feldman, V., 2011. *Spatial and temporal density dependence regulates the condition of central Baltic Sea clupeids: compelling evidence using an extensive international acoustic survey*. Popul. Ecol. 53, 511–523. https://doi.org/10.1007/s10144-011-0269-2

Chapman, R., 2006. *A sea water equation of state calculator*. APL Ocean Remote Sensing. http://fermi.jhuapl.edu/denscalc.html

Chu, D., Foote, K., Stanton T., 1993. *Further analysis of target strength measurements of Antarctic krill at 38 and 120 khz: Comparison with deformed cylinder model and inference of orientation distribution*. J. Acoust. Soc. Am. 93 (5), 2985–2988. https://doi.org/10.1121/1.405818

Didrikas, T., 2005. *Estimation of in situ target strength of the Baltic Sea herring and sprat*. Department of Systems Ecology. Stockholm University, 1 (5).

Didrikas, T., Hansson, S., 2004. *In situ target strength of the Baltic Sea herring and sprat*. ICES J. Mar. Sci. 61 (3), 378–382. https://doi.org/10.1016/j.icesjms.2003.08.003

Edwards, J.I., Armstrong, F., Magurran, A.E., Pitcher, T.J., 1984. *Herring, mackerel and sprat target strength experiments with behavioural observations*. ICES CM / B, 34.

Fässler, S.M.M., 2010. *Target strength variability in Atlantic herring (Clupea harengus) and its effect on acoustic abundance estimates*. PhD thesis, University of St. Andrews. https://doi.org/10.13140/2.1.1883.4247

Fässler, S.M.M., Gorska, N., 2009. *On the target strength of Baltic clupeids*. ICES J. Mar. Sci. 66, 1184–1190. https://doi.org/10.1093/icesjms/fsp005

Fässler, S.M.M., Gorska, N., Ona, E., 2007. *Differences in swimbladder volume between Baltic and Norwegian spring spawning herring: possible consequences for mean target strength*. ICES CM 2007/H, 3. https://doi.org/10.1016/j.fishres.2008.01.013

Fässler, S.M.M., Gorska, N., Ona, E., Fernandes, P.G., 2008. *Differences in swimbladder volume between Baltic and Norwegian spring-spawning herring: Consequences for mean target strength*. Fish. Res. 92, 314–321. https://doi.org/10.1016/j.fishres.2008.01.013

Fofonoff, N.P., Millard Jr, R.C., 1983. *Algorithms for the computation of fundamental properties of seawater*. UNESCO Publ., Paris. https://doi.org/10.25607/OBP-1450

Foote K.G., Francis D.T.I., 2002. *Comparing Kirchhoff-approximation and boundary-element models for computing gadoid target strengths*. J. Acoust. Soc. Am. 111, 1644–1654. https://doi.org/10.1121/1.1458939

Francis, D.T.I., 1993. *A gradient formulation of the Helmholtz integral equation for acoustic radiation and scattering*. J. Acoust. Soc. Am., 93, 1700–1709. https://doi.org/10.1121/1.406735

Francis, D.T.I., Foote, K.G., 2003. *Depth-dependent target strengths of gadoids by the boundary-element method*. J. Acoust. Soc. Am. 114, 3136–3146. https://doi.org/10.1121/1.1619982.

Fréon, P., Misund, O.A., 1999. *Dynamics of pelagic fish distribution and behaviour: effects on fisheries and stock assessment*. Vol. 348, Fishing News Books, Oxford.

Gaunaurd, G.C., 1985. *Sonar cross sections of bodies partially insonified by finite sound beams*. IEEE J. Ocean. Eng. 10, 213–230. https://doi.org/10.1109/JOE.1985.1145097

Gorska, N., 2007. *On target strength of Baltic herring*. ICES CM 2007/H 07, 17–21.

Gorska, N., Idczak, J., 2010. *On the acoustic backscattering by Baltic herring and sprat*. Hydroacoustics 13, 89–100. http://pta.eti.pg.gda.pl/journal/paper.py?id=469

Gorska, N., Idczak, J., 2021. *On Baltic herring morphometry and its impact on the backscattering properties*. Oceanologia, 64 (1), 198–211. https://doi.org/10.1016/j.oceano.2021.10.001

Gorska, N., Ona, E., 2003. *Modelling the acoustic effect of swimbladder compression in herring*. ICES J. Mar. Sci. 60, 548–554.

https://doi.org/10.1016/S1054-3139(03)00050-X

Grelowska, G., 2000. *Prevailing patterns of the sound speed distributions in the environment of the Southern Baltic*. Arch. Acoust. 25 (3).

Grygiel, W., Łączkowski, T., Podolska, M., Wodzinowski, T., 2011. *Research report from the Baltic International Acoustic Survey (BIAS) on board of the Polish r.v. Baltica (20.09–08.10.2010). Working paper on the WGBIFS meeting in Kaliningrad (Russia), 21–25.03.2011*. [in:] ICES CM 2011/SSGESST:05, REF. SCICOM, WGISUR, ACOM; Annex 9; 396–429.

Grygiel, W., Wyszyński, M., 2003. *Temporal (1980–2001) and geographic variation in the sexual maturity at age and length of herring and sprat inhabiting the southern Baltic*. Bull. Nat. Mar. Fish. Res. Inst. 159 (2), 3–34.

Hjellvik, V., Handegard, N.O., Ona, E., 2008. *Correcting for vessel avoidance in acoustic-abundance estimates for herring*. ICES J. Mar. Sci. 65 (6), 1036–1045. https://doi.org/10.1093/icesjms/fsn082

Holliday, D.V., 1972. *Resonance structure in echoes from schooled pelagic fish*. J. Acoust. Soc. Am. 51, 1322 –1332. https://doi.org/10.1121/1.1912978

Hornborg, S., 2023. *Follow the herring–A case study on the interplay between management and markets for marine resource utilization*. Mar. Policy 158, 105874. https://doi.org/10.1016/j.marpol.2023.105874

Huse, I., Korneliussen, R., 2000. *Diel variation in acoustic density measurements of overwintering herring (Clupea harengus L.)*. ICES J. Mar. Sci. 57 (4), 903–910. https://doi.org/10.1006/jmsc.2000.0577

Huse, I., Ona, E., 1996. *Tilt angle distribution and swimming speed of overwintering Norwegian spring spawning herring*. ICES J. Mar. Sci. 53 (5), 863–873. https://doi.org/10.1006/jmsc.1996.9999

ICES, 2017. *Manual for the International Baltic Acoustic Surveys (IBAS)*. Ser. ICES Survey Protocols SISP 8 – IBAS, Version 2.0, 47. http://www.ices.dk/sites/pub/Publication%20Reports/ICES%20Survey%20Protocols%20%28SISP%29/2017/SISP%208%20IBAS%202017.pdf

Idczak, J., Gorska, N., 2016. *Modelling of acoustic backscattering by southern Baltic herring*. Hydroacoustics 19, 145–152. http://pta.eti.pg.gda.pl/journal/paper.py?id=639

Idczak, J., Kniaź-Kubacka, N., 2012. *Backscattering properties of southern Baltic herring*. Hydroacoustics 15, 57–64. http://pta.eti.pg.gda.pl/journal/paper.py?id=531

Jaffe, J.S., Roberts, P.L., 2011. *Estimating fish orientation from broadband, limited-angle, multiview, acoustic reflections*. J. Acoust. Soc. Am. 129 (2), 670–680. https://doi.org/10.1121/1.3523430

Jech, J.M., Horne, J.K., Chu, D., Demer, D.A., Francis, D.T.I., Gorska, N., Jones, B., Lavery, A.C., Stanton, T.K., Macaulay, G.J., Reeder, D.B., Sawada, K., 2015. *Comparisons among ten models of acoustic backscattering used in aquatic ecosystem research*. J. Acoust. Soc. Am. 138, 3742–3764. https://doi.org/10.1121/1.4937607

Kasatkina, S., 2007. *Target strength of Baltic herring and sprat in relation to changes of their biological characteristics: effects on acoustic abundance indices estimates*. ICES CM /H, 06. https://doi.org/10.17895/ices.pub.25257874.v2

Kasatkina, S.M., 2009. *The influence of uncertainty in target strength on abundance indices based on acoustic surveys: examples of the Baltic Sea herring and sprat*. ICES J. Mar. Sci. 66, 1404–1409. https://doi.org/10.1093/icesjms/fsp086

Kloser, R., Ryan, T., Sakov, P., Williams, A., Koslow, J.A., 2002. *Species identification in deep water using multiple acoustic frequencies*. Can. J. Fish. Aquat. Sci. 59, 1065–1077.

Kulmala, S., Peltomäki, H., Lindroos, M., Söderkultalahti, P., Kuikka, S., 2007. *Individual transferable quotas in the Baltic Sea herring fishery: a socio-bioeconomic analysis*. Fish. Res. 84 (3), 368–377. https://doi.org/10.1016/j.fishres.2006.11.029

Lassen, H., Stæhr, K.J., 1985. *Target strength of Baltic herring and sprat measured in-situ*. ICES CM. B 41, 1–14.

Levine, I.N., 1978. *Physical Chemistry*. University of Brooklyn, McGraw-Hill.

Love, R.H., 1978. *Resonant acoustic scattering by swimbladder-bearing fish*. J. Acoust. Soc. Am. 64 (2), 571–580. https://doi.org/10.1121/1.382009

MacLennan, D.N., Fernandes, P.G., Dalen, J., 2002. *A consistent approach to definitions and symbols in fisheries acoustics*. ICES J. Mar. Sci. 59, 365–369. https://doi.org/10.1006/jmsc.2001.1158

Medwin, H., Clay, C.S., 1998. *Fundamentals of acoustical oceanography*. Acad. Press, New York, USA.

Mitson, R.B., (ed.) 1995. *Underwater Noise of Research Vessels: Review and Recommendations*. ICES Cooperative Res. Rep., 209 pp.

Mitson, R.B., Knudsen, H.P., 2003. *Causes and effects of underwater noise on fish abundance estimation*. Aquat. Living Resour. 16 (3), 255–263. https://doi.org/10.1016/S0990-7440(03)00021-4

Nakken, O., Olsen, K., 1977. *Target strength measurements of fish*. Rap. Proces. 170, 52–69.

Nero, R.W., Thompson, C.H., Jech, J.M., 2004. *In situ acoustic estimates of the swimbladder volume of Atlantic herring (Clupea harengus)*. ICES J. Mar. Sci. 61, 323–337.

Nøttestad, L., 1998. *Extensive gas bubble release in Norwegian spring spawning herring (Clupea harengus) during predator avoidance*. ICES J. Mar. Sci. 55 1133–1140. https://doi.org/10.1006/jmsc.1998.0416

Ojaveer, E., 1988. *Baltic Herrings. Biology and Management*. Agropromizdat, Moscow, Russia, 204 pp.

Olsen, K., Angell, J., Pettersen, F., Løvik, A., 1983. *Observed fish reactions to a surveying vessel with special reference to herring, cod, capelin and polar cod*. FAO Fish. 300, 131–138.

Ona, E., 1984. *Tilt angle measurements on herring*. ICES C.M. 1984/B, 19.

Ona, E., 1990. *Physiological factors causing natural variations in acoustic target strength of fish*. J. Mar. Biol. Assoc. UK 70, 107–127.

Ona, E., 2001. *Herring tilt angles, measured through target tracking*. [in:] *Herring: Expectations for a New Millennium*, 509–519.

Ona, E., Godø, O.R., Handegard, N.O., Hjellvik, V., Patel, R., Pedersen, G., 2007. *Silent research vessels are not quiet*. J. Acoust. Soc. Am. 121, 145–150. https://doi.org/10.1121/1.2710741

Pele, O., Werman, M., 2010. *The quadratic-chi histogram distance family*. [in:] *Computer Vision–ECCV 2010: 11th European Conference on Computer Vision, Heraklion, Crete, Greece, September 5–11, 2010 Proceedings, Part II*, Springer, Berlin, Heidelberg, 749–762.

Peltonen, H., Balk, H., 2005. *The acoustic target strength of herring (Clupea harengus L.) in the northern Baltic Sea*. ICES J. Mar. Sci. 62, 803–808. https://doi.org/10.1016/j.icesjms.2005.02.001

Rudstam, L.G., Hansson, S., Lindem, T., Einhouse, D.W., 1999. *Comparison of target strength distributions and fish densities obtained with split- and single-beam echosounders*. Fish. Res. 42, 207–214. https://doi.org/10.1016/S0165-7836(99)00047-8

Rudstam, L., Lindem, T., Hansson, S., 1988. *Density and in situ target strength of herring and sprat: a comparison between two methods of analyzing single beam sonar data*, Fish. Res. 6, 305–315. https://doi.org/10.1016/0165-7836(88)90001-X

Sawada, K., Furusawa, M., Williamson, N.J., 1993. *Conditions for the precise measurement of fish target strength in situ*. J. Mar. Acoust. Soc. Jpn. 20 (2), 73–79. https://doi.org/10.3135/jmasj.20.73

Sawicki, T., Juszczak, M., Szymczak, M., 2019. *Ichthyology and economic importance of baltic herring in polish fish industry*. Folia Pomeranae Universitatis Technologiae Stetinensis. Agricultura, Alimentaria, Piscaria et Zootechnica 348(49)1, 131–144. https://doi.org/10.21005/AAPZ2019.49.1.14

Scoulding, B., Chu, D., Ona, E., Fernandes, P.G., 2015. *Target strengths of two abundant mesopelagic fish species*. J. Acoust. Soc. Am. 137 (2), 989–1000. https://doi.org/10.1121/1.4906177

Scoulding, B., Gastauer, S., MacLennan, D.N., Fässler, S.M., Copland, P., Fernandes, P.G., 2017. *Effects of variable mean target strength on estimates of abundance: the case of Atlantic mackerel (Scomber scombrus)*. ICES J. Mar. Sci. 74 (3), 822–831. https://doi.org/10.1093/icesjms/fsw212

Scoulding, B., Chu, D., Ona, E., Fernandes, P.G. 2022. *Erratum: Target strengths of two abundant mesopelagic fish species*. J. Acoust. Soc. Am. 151, 3398. https://doi.org/10.1121/10.0011465

Simmonds, J., MacLennan, D.N., 2005. *Fisheries Acoustics: Theory and Practice*. 2nd Edn., Blackwell Publ., London.

Schmidt, B., Gorska, N., Szczucka, J., 2011. *Target strength relationship for herring and sprat in the southern Baltic Sea*. ICES 1129 Annual Science Conference, Gdańsk, Poland, 19–23 September, 2011, ICES Council Meeting 2011/R:15.

Stanton, T.K., 1988a. *Sound scattering by cylinders of finite length. I. Fluid cylinders*. J. Acoust. Soc. Am. 83, 55–63. https://doi.org/10.1121/1.396184

Stanton, T.K., 1988b. *Sound scattering by cylinders of finite length. II. Elastic cylinders*. J. Acoust. Soc. Am. 83, 64–67. https://doi.org/10.1121/1.396185

Stanton, T.K., 1989. *Sound scattering by cylinders of finite length. III. Deformed cylinders*. J. Acoust. Soc. Am. 86, 691–705. https://doi.org/10.1121/1.398193

Stanton, T.K., Reeder, D.B., Jech, J.M. 2003. *Inferring fish orientation from broadband-acoustic echoes*. ICES J. Mar. Sci. 60 (3), 524–531. https://doi.org/10.1016/S1054-3139(03)00032-8

Teacher, A.G., André, C., Jonsson, P.R., Merilä, J., 2013. *Oceanographic connectivity and environmental correlates of genetic structuring in Atlantic herring in the Baltic Sea*. Evol. Appl. 6 (3), 549–567. https://doi.org/10.1111/eva.12042

Thorne, R.E., Thomas, G.L., 1990. *Acoustic observations of gas bubble release by Pacific herring (Clupea harengus pallasi)*. Can. J. Fish. Aquat. Sci. 47, 1920–1928. https://doi.org/10.1139/f90-216

Martin Traykovski, L.V., O'Driscoll, R.L., McGehee, D.E., 1998. *Effect of orientation on broadband acoustic scattering of Antarctic krill Euphausia superba: Implications for inverting zooplankton spectral acoustic signatures for angle of orientation*. J. Acoust. Soc. Am. 104 (4), 2121–2135.

Vabø, R., Olsen, K., Huse, I., 2002. *The effect of vessel avoidance of wintering Norwegian spring spawning herring*. Fish. Res. 58, 59–77. https://doi.org/10.1016/S0165-7836(01)00360-5

Von Dorrien, C., Hammer, C., Zimmermann, C., Stepputtis, D., Stuermer, I.W., Kotterba, P., Polte, P., 2013. *A review on herring, Clupea harengus (Actinopterygii: Clupeiformes: Clupeidae) recruitment and early life stage ecology in the western Baltic Sea*. Acta Ichthyol. Piscat. 43, 169–182.

Wyszyński, M., 1997. *Charakterystyka biologiczno-technologiczna śledzia południowego Bałtyku*, Stud. Mat. Nat. Mar. Fish. Inst. Gdynia, Poland, Ser. B 69, 94–123.

Ye, Z., 1997. *Low-frequency acoustic scattering by gas-filled prolate spheroids in liquids*. J. Acoust. Soc. Am. 101 (4), 1945–1952. https://doi.org/10.1121/1.418225

Zampolli, M., Tesei, A., Jensen, F., Malm, N., Blottman, J., 2007. *A computationally efficient finite element model with perfectly matched layers applied to scattering from axially symmetric objects*. J. Acoust. Soc. Am. 122, 1472–1485. https://doi.org/10.1121/1.2764471

Żytko A., 2021. *Measurements and determination of fish orientation: Review of different methods*. [in:] Mieloszyk, M., Sagan, S., Ochrymiuk, T. (Eds.), *Selected problems in Earth and related environmental sciences*. Monogr. PAN, Wydawnictwo Instytutu Maszyn Przepływowych PAN.